SLAS Discovery 28 (2023) 376–384

Contents lists available at ScienceDirect

SLAS Discovery

journal homepage: www.elsevier.com/locate/slasd

Development of assays to support identification and characterization of modulators of DExH-box helicase DHX9

Deepali Gotur, April Case, Julie Liu, E. Allen Sickmier [1], Nicholas Holt, Kevin E. Knockenhauer, Shihua Yao, Young-Tae Lee, Robert A. Copeland, Shane M. Buker, P. Ann Boriack-Sjodin *

Accent Therapeutics, 1050 Waltham Street, Lexington, MA 02421, USA

ARTICLE INFO

Keywords:
DHX9
RNA helicase
DExH-box
Assay development
Drug discovery

ABSTRACT

DHX9 is a DExH-box RNA helicase that utilizes hydrolysis of all four nucleotide triphosphates (NTPs) to power cycles of 3′ to 5′ directional movement to resolve and/or unwind double stranded RNA, DNA, and RNA/DNA hybrids, R-loops, triplex-DNA and G-quadraplexes. DHX9 activity is important for both viral amplification and maintaining genomic stability in cancer cells; therefore, it is a therapeutic target of interest for drug discovery efforts. Biochemical assays measuring ATP hydrolysis and oligonucleotide unwinding for DHX9 have been developed and characterized, and these assays can support high-throughput compound screening efforts under balanced conditions. Assay development efforts revealed DHX9 can use double stranded RNA with 18-mer poly (U) 3′ overhangs and as well as significantly shorter overhangs at the 5′ or 3′ end as substrates. The enzymatic assays are augmented by a robust SPR assay for compound validation. A mechanism-derived inhibitor, GTPγS, was characterized as part of the validation of these assays and a crystal structure of GDP bound to cat DHX9 has been solved. In addition to enabling drug discovery efforts for DHX9, these assays may be extrapolated to other RNA helicases providing a valuable toolkit for this important target class.

1. Introduction

DHX9 (also known as RNA Helicase A (RHA) or Nuclear DNA Helicase II (NDH II); EC:3.6.4.13) is a versatile helicase capable of binding single stranded RNA and DNA, unwinding double stranded RNA and DNA, RNA-DNA hybrids and R-loops, as well as resolving more complex structures including triplex-DNA and G-quadraplexes (reviewed in [33]). DHX9 has been reported to have regulatory roles in a variety of cellular functions including DNA replication, transcription, translation, RNA processing and transport, microRNA processing and maintenance of genomic stability [21,33].

Consistent with its importance in multiple cellular functions, DHX9 has been implicated as a therapeutic target of interest in multiple disease areas. DHX9 has been identified as a dependency factor for multiple viruses (reviewed in [6]) including hepatitis B [13] and HIV-1 [5]. Genomic instability is a hallmark of cancer cells and targeting replication stress is an active area of investigation in oncology [16]. DHX9 prevents genomic instability caused by complex DNA structures including triplex-DNA [26] and loss of DHX9 promotes replication blockage caused by R-loops. This results in obstruction of DNA replication and thus increases genome instability [11]. *In vivo* studies utilizing an inducible RNAi platform targeting DHX9 showed that protein loss was detrimental to select tumor cells but otherwise well-tolerated in normal mouse tissue [32] indicating the potential of DHX9 inhibitors as a viable pathway for disease modulation.

DHX9 is a large, 1270 amino acid protein consisting of multiple domains whose biological functions have been well characterized [2,3,41,42,44]. It is a member of the SF2 helicase superfamily, which is defined by the presence of two RecA domains in the helicase core with conserved structural motifs. DHX9 also belongs to the DExH-box sub--family of helicases defined by the sequence Asp-Glu-x-His in motif II of the RecA domain 1 [20]. The structure of an N- and C-terminally truncated construct of MLE, the DHX9 ortholog in *Drosophila*, bound to a single stranded poly-U RNA and an ATP transition state analog, ADP-AlF_4, has been solved [37]. The structure revealed the RNA traverses thorough a well-defined globular protein; in addition, the nucleotide analog was bound in the expected position between the RecA1 and RecA2 domains. Recently, structures of three mammalian

* Corresponding author.
E-mail address: ABoriackSjodin@accenttx.com (P.A. Boriack-Sjodin).
[1] Present address: Recludix Pharma, Cambridge, MA, USA

https://doi.org/10.1016/j.slasd.2023.08.006
Received 6 June 2023; Received in revised form 2 August 2023; Accepted 22 August 2023
Available online 23 August 2023

DHX9 proteins bound to ADP have been reported and show the overall domain architecture observed in MLE to be conserved in higher species (PDB codes 8SZP, 8SZQ and 8SZR).

DExH-box helicases can bind and hydrolyze any NTP to unwind oligonucleotide substrates. Early reports utilizing human DHX9 from HeLa cells [31], bovine DHX9 purified from calf thymus [45] or recombinant *Drosophila melanogaster* MLE [30] confirmed full length DHX9 was active on both RNA and DNA and could utilize any NTP for unwinding activity [45]. Additional characterization of DHX9 activity on complex substrates [10] has also been performed. Structure-activity investigations into the domain structure of MLE showed the dsRBD2 domain was critical for unwinding activity but that the glycine-rich RGG motif and N-terminal dsRBD1 domain were dispensable [24,37]. Much of the characterization of DHX9 activity was performed using gel-shift assays to detect strand dissociation. Unfortunately, gel-based methods are unsuited for a high-throughput approach required for large-scale drug discovery efforts. Assays utilizing either hydrolysis of γ-^{32}P-ATP or detection of phosphate by malachite green have been developed for DHX9 in 96-well plate format [9]. However, miniaturization to 384-well format was not presented and kinetic characterization of the assays was not described.

In this report, a suite of assays capable of identifying and validating modulators of human DHX9 is presented. An *in vitro* assay monitoring ATP hydrolysis has been developed and optimized for high-throughput screening efforts. This assay was utilized to characterize DHX9 enzyme kinetics and optimal substrate concentrations were determined to enable compound screening under balanced conditions. Additionally, the first plate-based functional assay to measure compound effects on the ability of DHX9 to unwind double stranded oligonucleotides has been established. A robust SPR assay has been developed to confirm compounds identified in the enzymatic assays bind specifically to the protein and determine compound affinity. This suite of assays was utilized to validate and characterize GTPγS as a nucleotide-competitive inhibitor of DHX9 and a crystal structure of a mammalian DHX9 bound to GDP in the nucleotide binding site was solved. These assays provide a valuable toolkit for drug discovery efforts on DHX9.

2. Materials and methods

2.1. Reagents

RNA oligomers were synthesized by Integrated DNA Technologies (Coralville, IA) and purified by high-performance liquid chromatography (HPLC) to greater than 95% purity. Non-hydrolyzable nucleotide analogs were purchased from Jena Biosciences (Catalog # NK102; Jena, Germany). White, medium binding, polypropylene 384-well assay plates (Catalog #781075) and black, non-binding, polypropylene plates (Catalog #781075) were obtained from Greiner Bio-One (Frickenhausen, Germany) for the ATPase assay and helicase assay respectively. The ADP-Glo™ kinase assay kit (Catalog # V9102) was purchased from Promega Inc. and, in addition, supplied the ultra-pure ATP and ADP used in the experiments.

2.2. Protein production

All wild type constructs for human (*Homo sapiens*) DHX9 (UniProt entry: Q08211-1) or cat (*Felis sivestris catus*) DHX9 (UniProt entry: A0A337SGK2-1) were generated through subcloning from synthesized, full-length DHX9 DNA sequences that were codon optimized for protein overexpression. Human DHX9 (aa 150-1150-FLAG; referred to as hDHX9), avi-tagged human DHX9 (aa 150-1150-FLAG-Avi; referred to as hDHX9Avi) and cat DHX9 (aa 151-1151-FLAG; referred to as catDHX9) were each cloned into the pFastBac1 vector (Invitrogen). Human DHX9 with Asp 511 mutated Ala (hDHX9 D511A) was generated by PCR-based site-directed mutagenesis utilizing the Site-Directed Mutagenesis Kit (SDM-15, SBS Genetech) and hDHX9 as a template. Viral amplification was performed using standard procedures. For protein expression, Sf9 cells (2-2.5 $\times$ 10^6 cells/mL) were infected with virus at 1:100 ratio (v/v) and cultured for 72 h at 27 ℃. Cells were harvested by centrifugation and stored at -80 ℃ until purification. hDHX9 was purified by resuspending the cells in a binding buffer containing 25 mM HEPES, pH 7.5, 300 mM NaCl supplemented with protease inhibitor cocktail (Roche). After sonication and subsequent centrifugation to remove cell debris, the supernatant was added to anti-FLAG affinity gel (Sigma) pre-equilibrated with the binding buffer and incubated for 2 h at 4 ℃. The resin was washed three times sequentially with binding buffer, binding buffer with 5 mM ATP and 10 mM $MgCl_2$ and then binding buffer. The target protein was eluted by addition of 250 μg/mL FLAG peptide to the binding buffer. After elution of the protein from the FLAG resin, the protein was concentrated and a size exclusion column (Superdex 200, GE) was run using buffer containing 25 mM HEPES, pH 7.5 and 100 mM NaCl. The eluted protein was concentrated to $>$ 4 mg/mL, flash frozen in liquid nitrogen and stored at -80 ℃. SDS-page gel showed the final protein to be highly pure and SEC chromatography profile was consistent with a monomer (Supplemental Fig. S1A and S1B). The final protein yield for hDHX9 was 9 mg protein per 1 L of insect cell culture. The same purification method was used for hDHX9 D511A resulting in monomeric protein of high purity (Supplemental Fig. S1C and S1D) with final yields of 4.4 mg protein per 1 L insect cell culture.

CatDHX9 was purified in the same manner as hDHX9 except 2 mM TCEP was added to all buffers and the SEC column was run using a buffer containing 300 mM NaCl. SDS-page gel showed the final protein to be highly pure and SEC chromatography profile was consistent with a monomer (Supplemental Fig. S1E and S1F). The final protein yield for catDHX9 was 13.3 mg protein per 1 L of insect cell culture. hDHX9-Avi was purified by FLAG affinity in the same manner as hDHX9, with some modifications. After elution from the FLAG resin, the protein was biotinylated using a His-tagged BirA protein using methods previously established [12]. The protein solution was added to a nickel affinity column preincubated with binding buffer and hDHX9-Avi was eluted with binding buffer containing 20 mM imidazole. The protein was then purified by size exclusion chromatography in the same manner as hDHX9. SDS-page gel showed the final protein to be highly pure and SEC chromatography profile was consistent with a monomer (Supplemental Fig. S1G and S1H). The final protein yield for hDHX9 was 5.3 mg protein per 1 L of insect cell culture.

2.3. DHX9 ATPase assay

The DHX9 ATPase assay was performed in small-volume, medium binding, 384-well white plates at a final volume of 10 μL/well. Optimized 1X assay buffer was 40 mM HEPES (pH 7.5), 0.01% Tween 20, 0.01% BSA, 1 mM DTT, 20 mM $MgCl_2$, 0.004 U/ml RNAseOUT (cat. No. 10777019, Thermo Fisher Scientific). For nucleotide testing, DHX9 (final concentration (f.c.) = 0.625 nM) was added using a Multidrop Combi (Thermo Fisher Scientific) and preincubated for 15 min. Reactions were initiated by adding double stranded RNA substrate (f.c.= 15 nM) and ultra-pure ATP (f.c.= 5 μM) substrates. Reactions proceeded for 45 min and were stopped by the addition of ADP-Glo reagent. The reactions were then treated with Kinase Detection Reagent for 45 min. The plates were centrifuged at 800 rpm for 15 s and read on an Envision (PerkinElmer) plate-based reader for total luminescence signal.

2.4. DHX9 helicase assay

A DHX9 helicase assay was performed in small-volume, non-binding, 384-well black plates at a final volume of 20 μL/well. Optimized 1X assay buffer was 40 mM HEPES pH 7.5, 0.01% Tween 20, 0.01% BSA, 1 mM DTT, 20 mM $MgCl_2$, 0.004 U/ml RNAseOUT (cat. No. 10777019, Thermo Fisher Scientific). To test GTPγS, DHX9 ((f.c.) = 2.5 nM) and oligonucleotide (f.c.= 12.5 nM) were added into assay ready plates

containing the inhibitor using a Multidrop Combi (Thermo Fisher Scientific) and preincubated for 15 min. Reactions were started by adding Ultra-pure ATP (f.c.= 5 μM). An Envision plate reader (Perkin Elmer, Waltham, MA) with excitation and emission wavelengths set to 620 nm and 685 nm, respectively, was used to read the reaction kinetically at 60 s intervals for 30 min monitoring fluorescence signal. For kinetic analysis, raw fluorescence data was used calculate slopes by applying linear regression analysis to the linear phase of the reaction.

2.5. Biochemical assay data analysis

Enzyme kinetics and parameters such as K_M and k_{cat} were calculated using Michaelis–Menten fits of steady-state enzyme velocities in GraphPad (San Diego, CA). Scigillian Analyze software (Montreal, QC, Canada) was used to calculate IC_{50} values and Hill slopes using four-parameter fits. The quality and robustness of the assay were determined by analysis of the Z' factor. IC_{50} values for inhibitors were calculated from the midpoint values of concentration–response plots.

2.6. SPR assay development and data analysis

Surface Plasmon Resonance (SPR) binding studies were conducted using a Biacore S200 (Cytiva) at 20°C using 25 mM HEPES pH 7.5, 150 mM NaCl, 1.5 mM $MgCl_2$, 1 mM DTT, 5% glycerol, 0.005% Tween 20, +/- 1% DMSO as the running buffer. hDHX9-Avi protein was immobilized on a SA series S sensor chip (Cytiva). Prior to ligand immobilization, all flow cells were preconditioned by 3 consecutive injections of 50 mM NaOH in 1 M NaCl at 30 μL/min per manufacturer instructions. To immobilize several thousand response units of hDHX9-Avi on the SA chip, the protein was captured by injecting 20 μg/mL protein diluted in running buffer at 5 μL/min. The reference flow cell was left untreated. Analyte binding was tested in multicycle kinetic mode with 120 s association and 240 s dissociation at a flow rate of 30 μL/min. The data was solvent corrected when DMSO was included in the buffer and double reference subtracted using the streptavidin reference surface and a buffer blank injection. Competition experiments with ATP and ADP were run in A-B-A injection mode, where 100 μM ADP or ATP in running buffer served as solution A. Solution B was a titration series of GTPγS or GTP in solution A. Pre-sample contact time in solution A was 60 s, followed by 120 s for solution B, and 120 s post-sample contact time in solution A. Data were analyzed using the Biacore Insight Evaluation software (Cytiva) and curves were fit using the standard 1:1 binding kinetic model.

2.7. Crystallography

GDP was cocrystallized with catDHX9 using the hanging drop vapor diffusion method at 18°C. GDP was solubilized to 100 mM in water and added to catDHX9 (8 mg/ml) at a final concentration of 5 mM in a buffer containing 20 mM HEPES pH 7.5, 300 mM NaCl, 2 mM TCEP, and 50 mM $MgCl_2$. 1 μL of protein was added to 1 μL of precipitant solution containing 0.15 M ammonium sulfate, 0.1 M Tris, pH 8.2, 15% w/v PEG4000. A 0.5 mL reservoir was used for crystallization. Crystals were passed through a cryosolution containing 20% ethylene glycol and 80% precipitant solution prior to freezing in liquid nitrogen.

Diffraction data were collected at beamline BL45XU at Spring8. Data reduction and scaling were performed with XDS [28] and Aimless [19]. Structure determination was performed using the structure of ADP-bound catDHX9 (PDB code 8SZQ) and visual inspection of the electron density maps. The GDP dictionary was imported from the COOT monomers library and ligand fitting was performed manually in COOT [18]. Structure refinement was completed using iterative cycles of refinement and model building using REFMAC [34] and COOT [18], respectively. Validation of the refined structure was performed at the Protein Data Bank validation server (validate.wwpdb.org). Data collection and refinement statistics are shown in Table 1. The structure has been deposited in the Protein Data Bank (8SZS).

Table 1
Crystallographic data collection and refinement statistics.

Compound	GDP
Space group	$P4_32_12$
Cell constants:	
a, b, c (Å)	86.11, 86.11, 347.24
α, β, γ (°)	90.0, 90.0, 90.0
Resolution range (Å)	48.03-2.38
(Highest resolution shell)	(2.45-2.38)
Completeness overall (%)	100.0 (100.0)
Reflections, unique	53722
Multiplicity	26.1 (24.2)
I/σ	17.4 (2.4)
$R_{r.i.m}$ [1]	0.147 (1.561)
$R_{value\ overall}$ (%) [2]	0.220 (0.281)
$R_{value\ free}$ (%) [3]	0.265 (0.346)
Number of atoms:	
Non-hydrogen protein atoms	6817
Non-hydrogen ligand atoms (GDP)	28
Solvent molecules	294
R.M.S. deviations from ideal values	
Bond lengths (Å)	0.0022
Bond angles (°)	0.79
Average *B* values (Å^2)	
Protein all atoms	54.6
Ligand	47.4
Solvent	50.7
Φ, Ψ angle distribution for residues	
Most favoured regions (%)	98
In additional allowed regions (%)	2

[1] $R_{r.i.m.} = R_{merge}[N/(N-1)]^{1/2}$, where N = data multiplicity
[2] $R_{value} = \Sigma_{hkl}\ ||F_{obs}| - |F_{calc}|| / \Sigma_{hkl}\ |F_{obs}|$
[3] R_{free} is the cross-validation R factor computed for the test set of 5% of unique reflections

3. Results

3.1. DHX9 protein construct selection

Production of homogeneous, pure and biochemically active protein is an important component of assay development efforts. Human DHX9 is a relatively large protein with multiple domains critical to helicase enzyme function. Purification of full length DHX9 has been documented, but quantification of yields for the purification was not reported [44]. Several full length constructs with N- and/or C-terminal affinity tags for expression in eukaryotic systems were generated and tested for expression, but no full-length construct from either mammalian or insect cell expression methods produced protein of sufficient quality, quantity and purity to support assay development, subsequent hit finding and compound validation efforts (data not shown). The *Drosophila* DHX9 ortholog MLE containing the dsRBD2, L2, MTAD, RecA1, RecA2, HA2, OB and L3 linker domains (aa 105-1158) was previously shown to be enzymatically active [37]. Based on this information, a human DHX9 containing the equivalent residues (amino acids 150-1150) was generated. A construct containing a C-terminal FLAG tag was well expressed in insect cells and purified to homogeneity (Supplemental Fig. S1A). Size exclusion chromatography confirmed the protein eluted as a single peak (Supplemental Fig. S1B); the protein was 97.6% pure as measured by Bioanalyzer (Agilent, Santa Clara, CA). This construct, which was found to have ATPase activity using an ADP-Glo™ assay (Promega), was selected for further characterization and will be referred to as hDHX9 in this report.

3.2. Optimization and kinetic characterization of DHX9 ATPase assay

Initial activity characterization of hDHX9 utilized a buffer containing 40 mM HEPES (pH 7.5), 0.01% BSA, 1 mM DTT, 20 mM $MgCl_2$, 0.004 U/ml RNAseOUT, 1% DMSO (v/v), and substrate concentrations of 500 nM

and 500 μM for RNA and ATP, respectively. The ADP-Glo™ Kinase assay kit (Promega) provides a luminescent readout of ATP hydrolysis (Fig. 1A) and was used to quantify enzyme activity. The RNA substrate used for initial testing was a double stranded 31-mer with a single 5′ overhang (Fig. 1B). A DHX9 variant with a mutation in the Asp-Glu-x-His sequence in motif II, hDHX9 D511A, was tested for activity alongside the wild-type protein and found to be inactive, showing the ATPase activity seen in the reaction was specific to hDHX9 protein (Fig. 1C). Buffer optimization testing pH, detergents, ionic strength and reducing agents was performed with a focus on conditions appropriate for large-scale screening efforts. RNaseOUT (0.004 U/μL) was included to preserve RNA integrity at concentrations previously shown to be beneficial by mass spectrometry [8]. There was no significant change in enzyme activity between HEPES pH 6.5, 7.5, and 8.0; pH 7.5 was selected to best approximate physiological pH. Addition of either NaCl or KCl decreased activity even at relatively low concentrations (ie, 25 mM). Enzyme activity was dependent on addition of $MgCl_2$ although concentrations above 50 mM significantly reduced activity; 20 mM was selected as maximum activity was observed at this concentration. Detergent and protein carrier were desired in the final buffer to minimize potential nonspecific binding. Both Triton X-100 and Tween-20 detergents significantly improved enzyme activity but Tween-20 consistently showed higher activity than Triton X-100 at concentrations less than or equal to 0.01%. BSA was well tolerated in the assay. DMSO was tolerated up to 1% but sensitivity was seen at higher concentrations, providing an upper limit for this reagent for any future hit-finding efforts.

Using these optimized conditions, select double stranded RNA constructs differing with either one or three nucleotide 3′ sequence overhang as well as the single stranded RNA common to all duplex RNAs used (Fig. 1B) were tested for ATPase activity with DHX9 and compared with the activity of the single base 5′ overhang sequence using excess of both substrates (100 nM RNA and 100 μM ATP). Gel analysis of the RNA stock solutions indicated a majority of the three double stranded RNA samples were in duplex form (Supplemental Fig. S2) confirming any ATPase activity seen would be from the annealed substrate rather than single stranded RNA. The double stranded 31-mer RNA with a single nucleotide 5′ overhang provided optimum activation of ATPase activity while 1 or 3-base 3′ overhang RNAs had reduced activity and the single stranded RNA (ssRNA) had the lowest activity (Fig. 1D). With this information, assay development efforts continued with the 31-mer single base 5′ overhang double stranded RNA. Assay linearity was tested at multiple enzyme concentrations and at multiple timepoints. Reactions proceeded linearly for enzyme concentrations between 0.625 nM and 5 nM within the time course of the experiment, and 0.625 nM enzyme and a 45 min reaction time were selected (data not shown). Steady-state enzyme kinetic analysis was then performed by titrating either ATP or the dsRNA substrate at a fixed concentration of the other substrate. Multiple timepoints at each of these conditions were collected and initial velocities calculated from the linear region of the progress curves. Fitting of the data to the Michaelis-Menten equation yielded substrate K_M values for ATP and RNA of 5.1 ± 0.5 μM and 35 ± 8 nM, respectively (Fig. 1E and 1F). k_{cat} values derived from these experiments were similar at 46.6 ± 0.8 min^{-1} for ATP and 28.2 ± 1.8 min^{-1} for RNA. Final concentrations for RNA and ATP substrates within 2-fold of the K_M values, 15 nM and 5 μM respectively, were selected to run the assay under balanced conditions.

3.3. Optimization and kinetic characterization of DHX9 helicase assay

In addition to measurement of ATP hydrolysis, an assay to probe the functional unwinding activity of DHX9 was desired. Hanson *et al.* reported FRET-based fluorescence assays for measurement of hepatitis C virus helicase activity utilizing either a “split beacon” substrate (fluorophore and quencher on different oligonucleotide strands) or a “molecular beacon” substrate (fluorophore and quencher on the same oligonucleotide strand) [22]. Only the “split beacon” substrate was active with DHX9 and this methodology was adapted to develop a plate-based helicase assay (Fig. 2A). Oligonucleotides with sequences comparable to substrate in Hanson *et al.* were synthesized to incorporate a Cy5 fluorescent probe into an RNA strand and BHQ quencher into a DNA strand that could be annealed with the single stranded RNA to yield a double stranded substrate containing an 18 base 3′ poly(U) overhang (Fig. 2B, hereafter referred to as SB-RNA). The SB-RNA substrate was active in the hDHX9 helicase assay (Fig. 2C) and assay optimization was initiated. Identical buffer conditions as the ATPase assay were chosen to

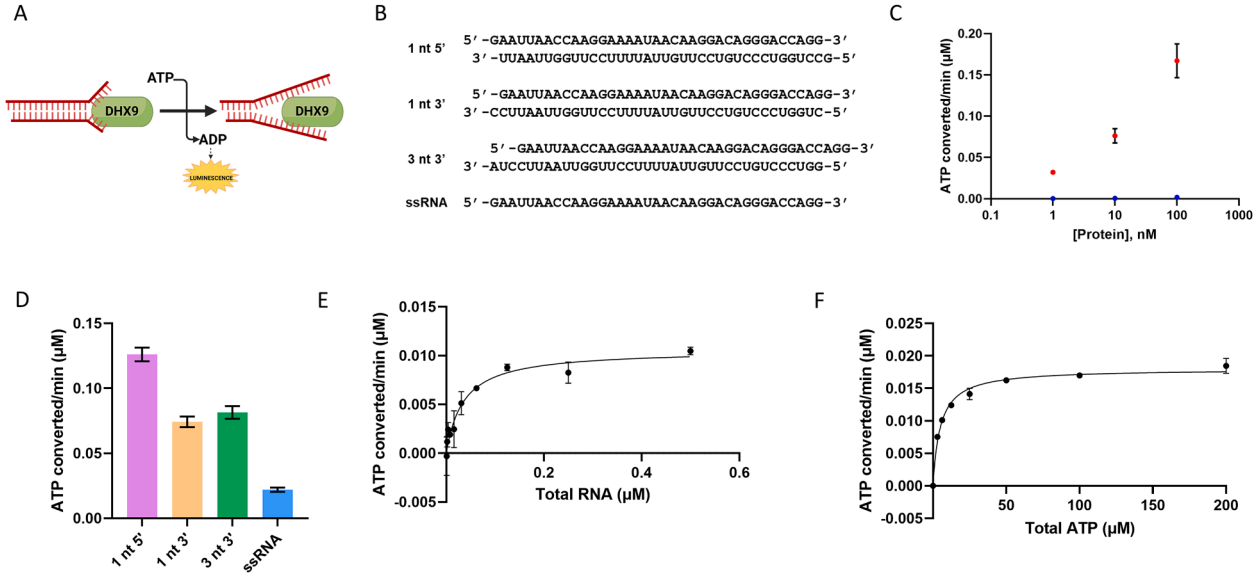

Fig. 1. Development and characterization of the DHX9 ATPase assay: A schematic of the assay is shown **(A)**. Multiple RNA constructs **(B)** were assembled for activity testing. Wild type hDHX9 (red) and variant hDHX9 D511A (blue) were tested for ATPase activity (n=3 technical replicates) **(C)**; only the wild type protein showed enzymatic activity. Single and double stranded RNAs were tested for ATPase activity (n=3 technical replicates) **(D)**. K_M values were determined for dsRNA **(E)** and ATP **(F)** using conditions described in the Materials and Methods section; n=2 biological replicates were performed with n=4 technical replicates contained within each K_M experiment.

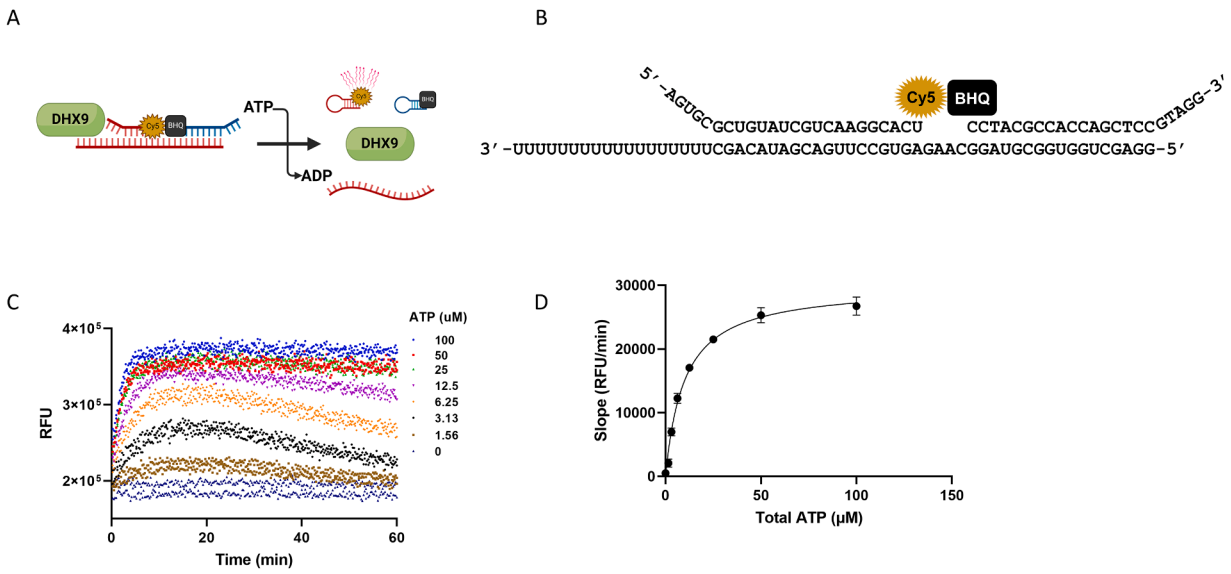

Fig. 2. Development and characterization of the DHX9 helicase assay: A schematic of the assay is shown **(A)**. The Cy5 moiety was incorporated into an RNA sequence and BHQ was incorporated into a DNA sequence; RNA was used as the complementary strand **(B)**. Example of raw fluorescence data generated by the helicase assay (n=2 technical replicates) **(C)**. ATP K_M was determined **(D)**; n=2 biological replicates were performed with n=3 technical replicates contained within each experiment.

directly compare ATPase and helicase activity. A K_M value of 9.9 ± 0.8 μM was measured for ATP in the helicase assay (Fig. 2D), but it was not possible to determine the K_M of the SB-RNA as the background fluorescence increased upon addition of increasing SB-RNA substrate. Theoretically, the SB-RNA substrate could be tested in the ATPase assay and RNA and ATP K_M values generated. However, in this case, the choice of Cy5 probe and BHQ quencher could be problematic as the wavelength of luminescent readout of the ADP-Glo assay (560 nm), the excitation wavelength of the Cy5 moiety in the SB-RNA construct (620 nm) and the quenching wavelength range of the BHQ group (480-580 nm) are close enough to cause interference and potentially skew resulting K_M values. Instead, the final concentration for the ATP substrate (5 μM) was selected based on the K_M value found for the helicase assay and the final RNA substrate concentration (12.5 nM) was chosen to closely match the duplex RNA concentration for the ATPase assay.

3.4. Development of DHX9 SPR assay

Development of an SPR assay for hDHX9 was desired as an orthogonal method to measure specific, reversible binding of compounds to the protein. The C-terminal avi-tagged hDHX9 protein (hDHX9-Avi) was captured on a streptavidin-coated chip. Buffer conditions were modified from the assay buffer conditions to enable robust delivery of compound data and minimize non-specific binding to the chip. Specifically, the salt concentration was increased, glycerol was added to the running buffer, the Tween-20 concentration was reduced and the protein components (BSA and RNaseOUT) were removed. Final buffer conditions were 25 mM HEPES pH 7.5, 150 mM NaCl, 1.5 mM $MgCl_2$, 1 mM DTT, 5% glycerol, 0.005% Tween and the hDHX9-Avi surface was stable under these optimized conditions. A 24 h stability study revealed the hDHX9-Avi surface lost only 15% of its starting binding activity (data not shown). Inclusion of 1% v/v DMSO was also well tolerated. To validate the assay, binding data were generated for the hDHX9-Avi substrate ATP and the product ADP. Both nucleotides bound comparably well to hDHX9-Avi, with K_D = 0.94 ± 0.25 μM for ATP and K_D = 0.40 ± 0.16 μM for ADP (Fig. 3A and 3B). Kinetic rate constants for substrate and product were also similar and comparable to K_M values determined in the ATPase and unwinding assays.

3.5. Identification and validation of GTPγS as an inhibitor of DHX9

Prior to initiation of large-scale hit finding efforts, validation of the hDHX9 assay suite was desired with a tool compound that would bind to DHX9 and inhibit enzymatic activity. The use of non-hydrolyzable ATP analogs as non-selective, active site inhibitors of kinases is well known and this same approach with ATP analogs has recently been applied to the bacterial helicase DnaB [29]. Unfortunately, the nature of substrate detection in the ATPase assay made non-hydrolysable ATP analogs untenable for this purpose due to the potential for high background caused by ATP and/or ADP contamination in the commercial material (data not shown). However, DHX9 can utilize NTP other than ATP to drive helicase activity [45] and the use of non-hydrolyzable analogs of other

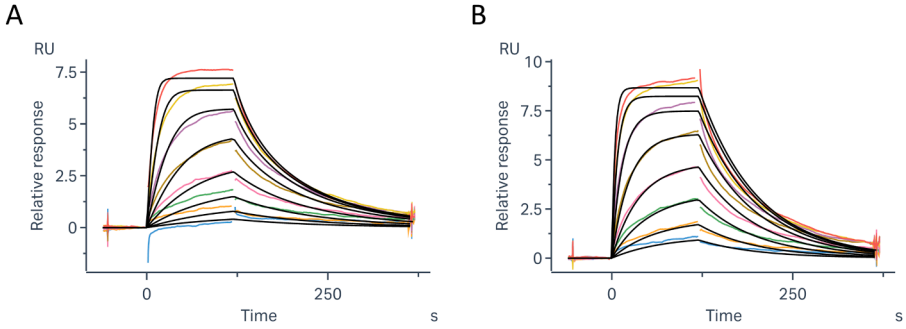

Fig. 3. Direct binding of nucleotides to DHX9 by Surface Plasmon Resonance: SPR sensorgrams in response to increasing concentrations of compound (color) and kinetic fits (black) flowed over immobilized Avi-hDHX9 are shown for ATP **(A)** and ADP **(B)**. Kinetic fit analysis determined K_D values of 0.94 ± 0.25 μM ($k_a = 1.1 \times 10^4\ M^{-1}\ s^{-1}$, $k_d = 9.9 \times 10^{-3}\ s^{-1}$) and 0.40 ± 0.16 μM ($k_a = 1.9 \times 10^4\ M^{-1}\ s^{-1}$, $k_d = 7.5 \times 10^{-3}\ s^{-1}$) for ATP and ADP respectively. Error reported as standard deviation. SPR experiments were performed in triplicate, representative sensorgrams shown.

nucleotides would not have the same issues in the biochemical assay due to the specificity of the assay detection for ADP rather than NDP. Therefore, characterization of the binding affinity of another NTP to DHX9 by SPR was performed. GTP was selected over other NTPs as it is also a purine nucleotide and could be expected to have similar affinity to DHX9. Indeed, binding of GTP to the enzyme showed equivalent affinity and kinetics to that of ATP (GTP K_D = 0.86 ± 0.35 μM; Fig. 4A). Furthermore, GTP binding was completely blocked upon addition of ATP in the buffer (Supplemental Fig. S3). Although expected, it was satisfying to see binding of an alternate NTP substrate in this assay with affinity equivalent to ATP and, presumably, in direct competition with ATP for the nucleotide binding site.

Since robust binding of GTP to hDHX9 observed by SPR, non-hydrolyzable analogs of GTP as well as the hydrolysis product, GDP, were tested for activity in the DHX9 ATPase assay (Fig. 4B). GTPγS was the most potent nucleotide, therefore, it was selected for additional assessment in the assay suite. When fully profiled, GTPγS was shown to have similar inhibitory activity in the ATPase assay (IC_{50} = 6.5 ± 0.7 μM; Fig. 4C) and the helicase assay (IC_{50} = 9.6 ± 3.9 μM; Fig. 4D). GTPγS also bound hDHX9-Avi as demonstrated by SPR (0.82 ± 0.15 μM; Fig. 4E). The binding of GTPγS was completely blocked upon addition of saturating levels of ADP in the buffer (Fig. 4F) indicating competitive binding to DHX9 for the two ligands. This result is consistent with binding of GTPγS in the ATP-binding site, as would be expected from a non-hydrolyzable analog of a DHX9 NTP substrate.

3.6. Crystal structure of GDP bound to DHX9

A structure of GTPγS bound to hDHX9 would be considered ideal to complete the validation package for this nucleotide analog as a DHX9 inhibitor. Crystal structures of human, cat and dog DHX9 orthologs with the same amino acid boundaries as hDHX9 have recently been reported with ADP bound in the nucleotide binding site (PDB codes 8SZP, 8SZQ and 8SZR for human, cat and dog, respectively) but to date, no structures of mammalian DHX9 bound to substrates or substrate analogs have been reported. Extensive crystallization screening with GTPγS was performed for this study, but no crystalline hits were identified and therefore no structure of GTPγS could be solved. Presumably, the conformation of DHX9 bound to the substrate analog, GTPγS, is incompatible with the packing interactions seen in the crystal system formed by the product ADP. This may be due to global changes in the three-dimensional structure of the DHX9 when bound to GTPγS which may be analogous to differences seen between the ADP-bound mammalian DHX9 structures and the RNA and/or ATP transition state-bound *Drosophila* MLE structures [25,37].

In an effort to determine if other nucleotide products could be solved in DHX9 in place of ADP using the known DHX9 crystal systems, cat DHX9 was cocrystallized in the presence of GDP which showed inhibitory activity in the initial screening of GTP analogs. This effort was successful and resulted in a 2.38 Å structure (Fig. 5A). The structure reveals the diphosphate nucleotide and a magnesium ion bound between the RecA1 and RecA2 domains, consistent with the previously reported ADP-bound structures. Although electron density maps at this resolution cannot distinguish between the carbonyl oxygen and amine nitrogen that differ between guanine and adenine bases at C6, the electron density maps clearly show the presence of the NH_2 group at the C2 position (Fig. 5B) which confirms the bound nucleotide as GDP. The guanine base is stacked between Arg 457 and Phe 700 (Fig. 5C) while the ribose and phosphate groups of GDP as well as the magnesium ion make several direct and water-mediated interactions with the protein (Fig. 5C and 5D). The structures of cat DHX9-GDP and cat DHX9-ADP (PDB code 8SZQ) co-complexes show high similarity with a C_α RMSD of 0.68 Å and the ADP and GDP nucleotides superimpose well in the nucleotide binding site (Fig. 5E). Consistent with the ability of DHX9 to utilize multiple NTP in its enzymatic activity, no hydrogen bonds are made between the base and the protein that could result in selectivity between substrates. This result is also concordant with the similar binding affinities seen for ATP and GTP by SPR.

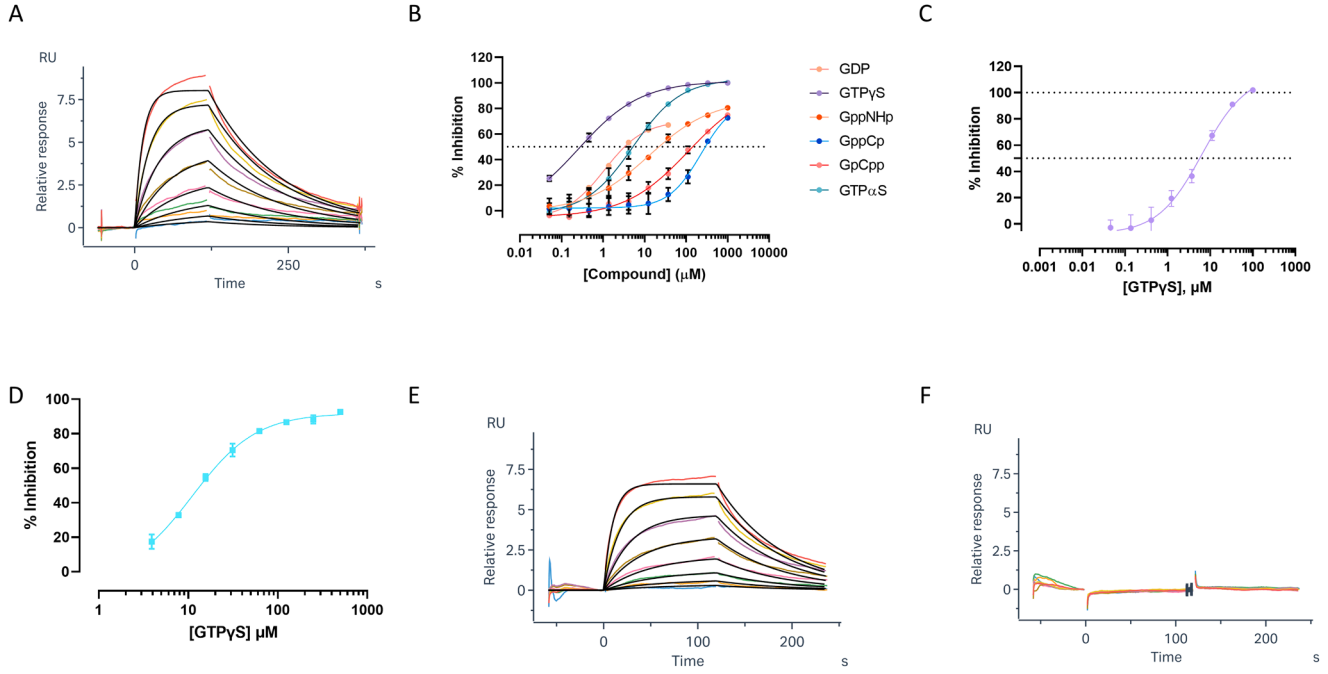

Fig. 4. Identification, validation and characterization of GTPγS as an inhibitor of DHX9: GTP binds DHX9 with a K_D value determined by kinetic fit analysis of of 0.86 ± 0.35 μM (k_a = 5.6 × 10^3 M^{-1} s^{-1}, k_d = 5.0 × 10^{-3} s^{-1}) **(A)**; error reported as standard deviation, triplicate experiments performed with a representative sensorgram shown. Nonhydrolyzable analogs of GTP and the product GDP were tested in the ATPase assay (n=2 technical replicates) **(B)**; GTPγS was selected for additional profiling. GTPγS IC_{50} values were determined using the ATPase assay (IC_{50} = 6.5 ± 0.7 μM (n=3 technical replicates)) **(C)** and the helicase assay (IC_{50} = 9.6 ± 3.9 μM (n=3 technical replicates)) **(D)**. SPR determined a K_D = 0.82 ± 0.15 μM (k_a = 6.2 × 10^3 1/Ms, k_d = 5.3 × 10^{-3} 1/s) (experiments performed in triplicate) **(E)**. A lack of dose response in SPR when ADP is in the buffer indicates GTPγS binding is fully blocked by the nucleotide **(F)**.

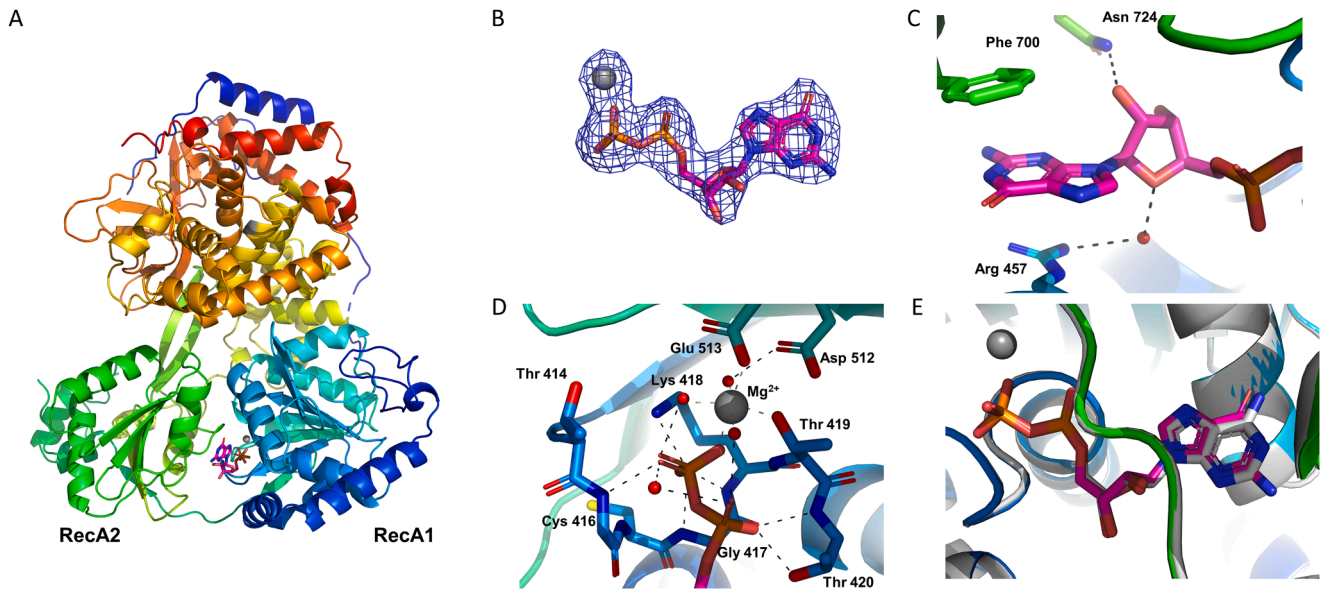

Fig. 5. Crystal structure of catDHX9 bound to GDP: **(A)** GDP (magenta) binds to catDHX9 (rainbow ribbon; N-terminus colored blue, C-terminus colored red) at the interface of the RecA1 and RecA2 domains. **(B)** An electron density map (Fo-Fc, 3.0 σ,) generated in the absence of GDP and magnesium shows clear density for the C6 amide of the guanine base. **(C)** The guanine base is in a π-stacking interaction with Arg 457 of RecA1 and Phe 700 of RecA2 and the ribose makes hydrogen bonding interactions (black dashed lines) with Asn 724 and water (red spheres). **(D)** Multiple hydrogen bonds are made between the GDP phosphate oxygen atoms and amino acids 414-420 and magnesium is coordinated by water molecules and the side chains of Glu 513 and Thr 419 (grey dashed lines). **(E)** Crystal structures of catDHX9 bound to GDP or ADP (light grey) superimpose well with respect to both protein and ligand.

4. Discussion

Helicases play an important role in a variety of critical cellular functions and RNA helicases are increasingly seen as important targets for drug discovery efforts. However, development of potent and selective inhibitors of RNA helicases has been challenging [1]. DHX9 plays critical roles in multiple cellular functions, including maintenance of genomic stability. Notwithstanding the clinical importance of this target enzyme, no selective inhibitors of DHX9 are currently known. Development of a suite of assays to enable compound screening is an important step in initial drug discovery efforts. Biochemical and biophysical assays as well as crystallography efforts were critical in the identification, validation, and optimization of inhibitors for the DNA helicase SMARCA2 [36].

The plate-based ATPase assay presented here is the first to be reported for DHX9 utilizing a double stranded RNA, and the helicase assay is the first plate-based assay capable of measuring the unwinding activity of the enzyme. Previous plate-based ATPase assays for DHX9 utilized single stranded poly(U) RNA to stimulate ATPase activity and development of an unwinding assay was unsuccessful due to an insufficient signal-to-noise window [9]. In this report, ssRNA stimulates ATP hydrolysis but it does so less effectively than the double stranded RNA substrates presented in this report. It is unknown if the full ensemble of conformational states of the enzyme is sampled in the absence of the double stranded or more structurally complex substrates. Utilizing double stranded substrates in the ATPase assay ensures all conformations required for unwinding activity are sampled during compound screening, although conformational states sampled only when DHX9 is bound to more complex substrates, such as triplex DNA or G-quadruplexes, could be missed. Importantly, the ability to measure the modulation of both the ATPase and RNA unwinding by DHX9 provides a valuable assessment of whether any inhibitors of the *in vitro* ATPase activity may also be inhibitors of the functional activity in cells.

Development of a DHX9 assay under conditions when both nucleotide and RNA substrate concentrations are close to K_M values is preferred for screening large diversity libraries. These conditions provide an equal likelihood of identifying inhibitors with differing interaction modalities with the target enzyme [14,15]. The use of malachite green as a detection method may be the reason substrate concentrations well above K_M values (2.5 μM RNA and 2 mM nucleotide) were used previously in plate-based DHX9 assays [9]. The malachite green detection reagent is able to detect 1 μM inorganic phosphate [23] while the ADP-Glo assay can measure 1 pM ADP [43]. Hydrolysis of ATP produces both ADP and inorganic phosphate, therefore, the use of the Promega ADP-Glo kit provides increased sensitivity for ATP hydrolysis over other phosphate detection methods, enabling a reasonable signal window with low nanomolar concentrations of enzyme and RNA substrate. However, the concentrations of RNA are significantly lower than typical concentrations of compounds used for screening efforts (1-30 μM). This concentration difference could result in a significant number of false positive compound hits if the compounds inhibit the assay by binding, precipitating or otherwise inactivating the RNA substrate used in the assay. To filter out such false positive compounds, an assay measuring binding of compounds directly to the double stranded RNA could be applied after initial screening efforts. An assay measuring intercalation of a fluorescent intercalator with DNA has been described for the DNA helicase, WRN, specifically to identify these types of compounds [4] and can be adapted for DHX9.

DExH-box helicases typically require the presence of a 3′ overhang for unwinding activity [27,35,38]. In this report, the ATPase activity of double stranded RNA substrates was significantly higher than single stranded RNA and the 5′ single base overhang was the most active of the limited number of double stranded RNAs tested. In studies of Drosophila MLE with an equivalent protein construct [37], MLE was active on RNA constructs with 10 uridine 3′ overhangs but unable to unwind RNA constructs with 10 uridine 5′ overhangs. However, MLE was also able to unwind blunt-ended RNA duplexes, albeit less efficiently than RNA molecules with longer 3′ overhangs, a characteristic that was seen as unique among DExH helicases. Given the significant amount of ATPase activity for duplex RNA substrates containing short 5′ or 3′ overhangs, it appears DHX9 is capable of utilizing these short, single base overhangs for hydrolysis of ATP. Therefore, it can be inferred that DHX9 shares this unique characteristic of unwinding blunt-ended or near-blunt ended substrates with MLE. A comprehensive and quantitative study of DHX9

substrate preference has not been performed in this study which was instead focused on developing an assay suite suitable for enabling drug discovery efforts for DHX9. For this application, the use of a double stranded RNA as the DHX9 substrate was preferred over single stranded oligonucleotides due to the varied nature of DHX9 cellular substrates. However, the assays presented in this report provide a cogent platform with which to characterize fully the impact of oligonucleotide type (RNA, DNA or hybrid), duplex length, overhang length, orientation, sequence and other oligonucleotide variables on binding and enzyme turnover by measuring differences in K_M and k_{cat} for each potential substrate in both the ATPase assay and unwinding assay. This level of quantification and mechanistic detail is not possible with gel-based and like methods, although close attention to the excitation wavelength of any probe or quencher group absorbance range for labeled RNA should be noted to ensure interference with ATPase luminescence signal is avoided. Additionally, the assays presented here may be adapted to other helicases for similar investigations.

Identification of a specific, reversible tool compound is an important validation step during assay development. However, the use of non-hydrolysable ATP analogs as specific, non-selective tool inhibitors of *in vitro* activity as was shown for the bacterial helicase DnaB [29] was not possible due to increased background in the ATPase assay (data not shown), presumably from adenine-based contaminants. As a member of the DExH-box helicase subfamily, DHX9 can utilize all NTP as substrates, not just ATP. This NTP promiscuity of the enzyme and determination of the low μM binding affinity of GTP to hDHX9 by SPR was exploited to select a non-hydrolyzable analog of GTP, GTPγS, as a potential inhibitor of DHX9 ATP hydrolysis without compromising assay fidelity. Indeed, this approach proved to be successful as GTPγS was found to be an inhibitor of the enzyme ATPase activity and helicase activity as well as bind to DHX9 by SPR with low micromolar potency.

It has been noted that inhibitors that bind to the nucleotide binding site of RNA helicases may not be preferred for drug discovery due to conservation across family members and the potential for cross-reactivity with other enzymes [39]. While competitive inhibitors for the nucleotide binding site will be identified under balanced screening conditions, these can be rapidly categorized using enzymatic methodologies [7] and/or SPR methods using saturating concentrations of ATP or other nucleotides. In this study, as expected given the mechanism-guided methodology used to identify the compound, SPR methods unambiguously identified GTPγS as a competitive inhibitor of ATP. Given these results, this suite of biochemical and biophysical assays can be utilized to characterize additional nucleotide analogs or identify and validate non-nucleotide small molecule inhibitors of DHX9 that may be more suitable for drug discovery objectives.

A crystal structure of GTPγS bound to DHX9 in the nucleotide binding site would have provided unambiguous evidence for the inhibition of activity due to binding in the active site of the molecule. Unfortunately, a crystal structure with GTPγS could not be obtained. Instead, efforts were undertaken to cocrystallize GDP with DHX9 using the same crystal system utilized for the structure of cat DHX9 with ADP (PDB code 8SZQ) to see if the published conditions could be repeated with a similar compound, in this case, another nucleotide hydrolysis product. This effort was successful as the resulting electron density maps clearly showed binding of GDP in the nucleotide binding site, providing a second structure of a nucleotide diphosphate bound to a mammalian DHX9. The ATPase and helicase assays presented in this report sample all conformations of DHX9 required for ATP hydrolysis and substrate unwinding. Therefore, an inhibitor of DHX9 activity found using the assays presented in this report may bind to any conformational state of DHX9 sampled during the reaction process; alternatively, a compound may induce a new conformation of the DHX9 protein upon binding. The biochemical and biophysical experiments presented here can be used to inform on the appropriate use of substrates or other ligands to utilize in crystallization screening when seeking to obtain structural validation of a compound identified in a screening campaign. This information is critical to maximize the potential for enablement of structure-based design efforts and will be particularly valuable for a target with significant structural movements as part of its enzymatic mechanism such as DHX9. That said, it remains to be seen if the product-bound conformation of DHX9, captured in the ADP and GDP structures, will be useful for the validation of any compounds identified through screening efforts.

As a target class, helicases can provide unique challenges for inhibitor identification and optimization [17,40]. Screening of large diversity libraries requires robust, high-throughput, plate-based assays optimized for compound screening efforts. Validation and characterization of hits identified by screening requires orthogonal assays to ensure only specific inhibitors of enzyme function are advanced. The assays for DHX9 presented here provide a toolkit for initiation of drug discovery efforts on this enzyme, an opportunity to investigate substrate specificity for this unique DExH-box helicase and a framework for the development of biochemical assays for other helicases of biological interest.

Declaration of Competing Interest

The authors declare the following financial interests/personal relationships which may be considered as potential competing interests:

P. Ann Boriack-Sjodin reports a relationship with Accent Therapeutics, Inc that includes: equity or stocks. Young-Tae Lee reports a relationship with Accent Therapeutics, Inc that includes: equity or stocks. E. Allen Sickmier reports a relationship with Accent Therapeutics, Inc that includes: equity or stocks. Deepali Gotur reports a relationship with Accent Therapeutics, Inc that includes: equity or stocks. April Case reports a relationship with Accent Therapeutics, Inc that includes: equity or stocks. Julie Liu reports a relationship with Accent Therapeutics, Inc that includes: equity or stocks. Nicholas Holt reports a relationship with Accent Therapeutics, Inc that includes: equity or stocks. Kevin E. Knockenhauer reports a relationship with Accent Therapeutics, Inc that includes: equity or stocks. Shihua Yao reports a relationship with Accent Therapeutics, Inc that includes: equity or stocks. Robert A. Copeland reports a relationship with Accent Therapeutics, Inc that includes: equity or stocks. Shane M. Buker reports a relationship with Accent Therapeutics, Inc that includes: equity or stocks.

Acknowledgements

The authors wish to thank Yu Xia for coordination of protein production and structural biology efforts, Natalie Klug, Huawen Lin, and Jeff Hirsh for help with helicase assay development, and Jennifer Castro, Matthew Daniels and Simina Grigoriu for helpful discussions.

Supplementary materials

Supplementary material associated with this article can be found, in the online version, at doi:10.1016/j.slasd.2023.08.006.

References

[1] Abdelkrim YZ, Banroques J, Kyle Tanner N. Known inhibitors of RNA helicases and their therapeutic potential. In: Boudvillain M, editor. RNA remodeling proteins, methods in molecular biology. New York, NY: Springer US; 2021. p. 35–52. https://doi.org/10.1007/978-1-0716-0935-4_3.

[2] Aratani S, Fujii R, Oishi T, Fujita H, Amano T, Ohshima T, Hagiwara M, Fukamizu A, Nakajima T. Dual roles of RNA helicase A in CREB-dependent transcription. Mol Cell Biol 2001;21:4460–9. https://doi.org/10.1128/MCB.21.14.4460-4469.2001.

[3] Aratani S, Oishi T, Fujita H, Nakazawa M, Fujii R, Imamoto N, Yoneda Y, Fukamizu A, Nakajima T. The nuclear import of RNA helicase A is mediated by importin-α3. Biochem Biophys Res Commun 2006;340:125–33. https://doi.org/10.1016/j.bbrc.2005.11.161.

[4] Banerjee T, Aggarwal M, Sommers JA, Brosh RM. Biochemical and cell biological assays to identify and characterize DNA helicase inhibitors. Methods 2016;108:130–41. https://doi.org/10.1016/j.ymeth.2016.04.007.

[5] Bolinger C, Sharma A, Singh D, Yu L, Boris-Lawrie K. RNA helicase A modulates translation of HIV-1 and infectivity of progeny virions. Nucleic Acids Res 2010;38:1686–96. https://doi.org/10.1093/nar/gkp1075.

[6] Bonaventure B, Goujon C. DExH/D-box helicases at the frontline of intrinsic and innate immunity against viral infections. J Gen Virol 2022;103. https://doi.org/10.1099/jgv.0.001766.

[7] Buker SM, Boriack-Sjodin PA, Copeland RA. Enzyme–inhibitor interactions and a simple, rapid method for determining inhibition modality. SLAS Discov 2019;24:515–22. https://doi.org/10.1177/2472555219829898.

[8] Buker SM, Gurard-Levin ZA, Wheeler BD, Scholle MD, Case AW, Hirsch JL, Ribich S, Copeland RA, Boriack-Sjodin PA. A mass spectrometric assay of METTL3/METTL14 methyltransferase activity. SLAS Discov 2020;25:361–71. https://doi.org/10.1177/2472555219878408.

[9] Cencic R, Senechal P, Pelletier J. Establishment of a primary screening assay for the DHX9 helicase. CCHTS 2015;18:855–61. https://doi.org/10.2174/1386207318666151019093433.

[10] Chakraborty P, Grosse F. Human DHX9 helicase preferentially unwinds RNA-containing displacement loops (R-loops) and G-quadruplexes. DNA Repair 2011;10:654–65. https://doi.org/10.1016/j.dnarep.2011.04.013.

[11] Chakraborty P, Huang JTJ, Hiom K. DHX9 helicase promotes R-loop formation in cells with impaired RNA splicing. Nat Commun 2018;9:4346. https://doi.org/10.1038/s41467-018-06677-1.

[12] Chan-Penebre E, Kuplast KG, Majer CR, Boriack-Sjodin PA, Wigle TJ, Johnston LD, Rioux N, Munchhof MJ, Jin L, Jacques SL, West KA, Lingaraj T, Stickland K, Ribich SA, Raimondi A, Scott MP, Waters NJ, Pollock RM, Smith JJ, Barbash O, Pappalardi M, Ho TF, Nurse K, Oza KP, Gallagher KT, Kruger R, Moyer MP, Copeland RA, Chesworth R, Duncan KW. A selective inhibitor of PRMT5 with *in vivo* and *in vitro* potency in MCL models. Nat Chem Biol 2015;11:432–7. https://doi.org/10.1038/nchembio.1810.

[13] Chen Y, Shen B, Zheng X, Long Q, Xia J, Huang Y, Cai X, Wang D, Chen J, Tang N, Huang A, Hu Y. DHX9 interacts with APOBEC3B and attenuates the anti-HBV effect of APOBEC3B. Emerg Microbes Infect 2020;9:366–77. https://doi.org/10.1080/22221751.2020.1725398.

[14] Copeland RA. Evaluation of enzyme inhibitors in drug discovery: a guide for medicinal chemists and pharmacologists. 2nd ed. Hoboken, N.J: Wiley; 2013.

[15] Copeland RA. Mechanistic considerations in high-throughput screening. Anal Biochem 2003;320:1–12. https://doi.org/10.1016/S0003-2697(03)00346-4.

[16] da Costa AABA, Chowdhury D, Shapiro GI, D'Andrea AD, Konstantinopoulos PA. Targeting replication stress in cancer therapy. Nat Rev Drug Discov 2023;22:38–58. https://doi.org/10.1038/s41573-022-00558-5.

[17] Datta A, Brosh RM. New insights into DNA helicases as druggable targets for cancer therapy. Front Mol Biosci 2018;5:59. https://doi.org/10.3389/fmolb.2018.00059.

[18] Emsley P, Lohkamp B, Scott WG, Cowtan K. Features and development of *Coot*. Acta Crystallogr D Biol Crystallogr 2010;66:486–501. https://doi.org/10.1107/S0907444910007493.

[19] Evans PR, Murshudov GN. How good are my data and what is the resolution? Acta Crystallogr D Biol Crystallogr 2013;69:1204–14. https://doi.org/10.1107/S0907444913000061.

[20] Fairman-Williams ME, Guenther UP, Jankowsky E. SF1 and SF2 helicases: family matters. Curr Opin Struct Biol 2010;20:313–24. https://doi.org/10.1016/j.sbi.2010.03.011.

[21] Gulliver C, Hoffmann R, Baillie GS. The enigmatic helicase DHX9 and its association with the hallmarks of cancer. Future Sci OA 2020;7:FSO650. https://doi.org/10.2144/fsoa-2020-0140.

[22] Hanson AM, Hernandez JJ, Shadrick WR, Frick DN. Identification and analysis of inhibitors targeting the hepatitis C virus NS3 helicase. Methods in enzymology. Elsevier; 2012. p. 463–83. https://doi.org/10.1016/B978-0-12-396546-2.00021-8.

[23] Itaya K, Ui M. A new micromethod for the colorimetric determination of inorganic phosphate. Clin Chim Acta 1966;14:361–6. https://doi.org/10.1016/0009-8981(66)90114-8.

[24] Izzo A, Regnard C, Morales V, Kremmer E, Becker PB. Structure-function analysis of the RNA helicase maleless. Nucleic Acids Res 2008;36:950–62. https://doi.org/10.1093/nar/gkm1108.

[25] Jagtap PKA, Müller M, Kiss AE, Thomae AW, Lapouge K, Beck M, Becker PB, Hennig J. Structural basis of RNA-induced autoregulation of the DExH-type RNA helicase maleless. bioRxiv 2022. https://doi.org/10.1101/2022.11.11.516098.

[26] Jain A, Bacolla A, del Mundo IM, Zhao J, Wang G, Vasquez KM. DHX9 helicase is involved in preventing genomic instability induced by alternatively structured DNA in human cells. Nucleic Acids Res 2013;41:10345–57. https://doi.org/10.1093/nar/gkt804.

[27] Jankowsky E. RNA helicases at work: binding and rearranging. Trends Biochem Sci 2011;36:19–29. https://doi.org/10.1016/j.tibs.2010.07.008.

[28] Kabsch W. XDS. Acta Crystallogr D Biol Crystallogr 2010;66:125–32. https://doi.org/10.1107/S0907444909047337.

[29] Lacabanne D, Wiegand T, Wili N, Kozlova MI, Cadalbert R, Klose D, Mulkidjanian AY, Meier BH, Böckmann A. ATP analogues for structural investigations: case studies of a DnaB helicase and an ABC transporter. Molecules 2020;25:5268. https://doi.org/10.3390/molecules25225268.

[30] Lee CG, Chang KA, Kuroda MI, Hurwitz J. The NTPase/helicase activities of Drosophila maleless, an essential factor in dosage compensation. EMBO J 1997;16:2671–81. https://doi.org/10.1093/emboj/16.10.2671.

[31] Lee CG, Hurwitz J. A new RNA helicase isolated from HeLa cells that catalytically translocates in the 3 to 5 direction. J Biol Chem 1992;267:4398–407.

[32] Lee T, Paquet M, Larsson O, Pelletier J. Tumor cell survival dependence on the DHX9 DExH-box helicase. Oncogene 2016;35:5093–105. https://doi.org/10.1038/onc.2016.52.

[33] Lee T, Pelletier J. The biology of DHX9 and its potential as a therapeutic target. Oncotarget 2016;7:42716–39. https://doi.org/10.18632/oncotarget.8446.

[34] Murshudov GN, Vagin AA, Dodson EJ. Refinement of macromolecular structures by the maximum-likelihood method. Acta Crystallogr D Biol Crystallogr 1997;53:240–55. https://doi.org/10.1107/S0907444996012255.

[35] Ozgur S, Buchwald G, Falk S, Chakrabarti S, Prabu JR, Conti E. The conformational plasticity of eukaryotic RNA-dependent ATPases. FEBS J 2015;282:850–63. https://doi.org/10.1111/febs.13198.

[36] Papillon JPN, Nakajima K, Adair CD, Hempel J, Jouk AO, Karki RG, Mathieu S, Möbitz H, Ntaganda R, Smith T, Visser M, Hill SE, Hurtado FK, Chenail G, Bhang H-EC, Bric A, Xiang K, Bushold G, Gilbert T, Vattay A, Dooley J, Costa EA, Park I, Li A, Farley D, Lounkine E, Yue QK, Xie X, Zhu X, Kulathila R, King D, Hu T, Vulic K, Cantwell J, Luu C, Jagani Z. Discovery of orally active inhibitors of Brahma Homolog (BRM)/SMARCA2 ATPase activity for the treatment of brahma related gene 1 (BRG1)/SMARCA4-mutant cancers. J Med Chem 2018;61:10155–72. https://doi.org/10.1021/acs.jmedchem.8b01318.

[37] Prabu JR, Müller M, Thomae AW, Schüssler S, Bonneau F, Becker PB, Conti E. Structure of the RNA helicase MLE reveals the molecular mechanisms for uridine specificity and RNA-ATP coupling. Mol Cell 2015;60:487–99. https://doi.org/10.1016/j.molcel.2015.10.011.

[38] Pyle AM. Translocation and unwinding mechanisms of RNA and DNA helicases. Annu Rev Biophys 2008;37:317–36. https://doi.org/10.1146/annurev.biophys.37.032807.125908.

[39] Radi M, Falchi F, Garbelli A, Samuele A, Bernardo V, Paolucci S, Baldanti F, Schenone S, Manetti F, Maga G, Botta M. Discovery of the first small molecule inhibitor of human DDX3 specifically designed to target the RNA binding site: towards the next generation HIV-1 inhibitors. Bioorg Med Chem Lett 2012;22:2094–8. https://doi.org/10.1016/j.bmcl.2011.12.135.

[40] Shadrick WR, Ndjomou J, Kolli R, Mukherjee S, Hanson AM, Frick DN. Discovering new medicines targeting helicases: challenges and recent progress. SLAS Discov 2013;18:761–81. https://doi.org/10.1177/1087057113482586.

[41] Xing L, Niu M, Kleiman L. Role of the OB-fold of RNA helicase A in the synthesis of HIV-1 RNA. Biochim Biophys Acta (BBA) Gene Regul Mech 2014;1839:1069–78. https://doi.org/10.1016/j.bbagrm.2014.08.008.

[42] Xing L, Zhao X, Niu M, Kleiman L. Helicase associated 2 domain is essential for helicase activity of RNA helicase A. Biochim Biophys Acta (BBA) Proteins Proteom 2014;1844:1757–64. https://doi.org/10.1016/j.bbapap.2014.07.001.

[43] Zegzouti H, Zdanovskaia M, Hsiao K, Goueli SA. ADP-Glo: a bioluminescent and homogeneous ADP monitoring assay for kinases. Assay Drug Dev Technol 2009;7:560–72. https://doi.org/10.1089/adt.2009.0222.

[44] Zhang S, Grosse F. Domain structure of human nuclear DNA helicase II (RNA Helicase A). J Biol Chem 1997;272:11487–94. https://doi.org/10.1074/jbc.272.17.11487.

[45] Zhang S, Grosse F. Nuclear DNA helicase II unwinds both DNA and RNA. Biochemistry 1994;33:3906–12. https://doi.org/10.1021/bi00179a016.